Atomic scale analysis of defect clustering and predictions of their concentrations in UO_{2+x}

Emre Caglak[1,2,,†], Kevin Govers[2,‡], Dirk Lamoen[3], Pierre-Etienne Labeau[1], Marc Verwerft[2]*

[1]Université Libre de Bruxelles, Service de Métrologie Nucléaire, CP 165/84, 50 av. F.D. Roosevelt, B-1050 Brussels, Belgium

[2]Belgian Nuclear Research Centre, SCK CEN, Nuclear Materials Science Institute, Boeretang 200, B-2400 Mol, Belgium

[3]EMAT, Department of Physics, Universiteit Antwerpen, Groenenborgerlaan 171, 2020 Antwerpen, Belgium.

** Corresponding Author: emre.caglak@ulb.ac.be*

Abstract

The physical properties of uranium dioxide vary greatly with stoichiometry. Oxidation towards hyperstoichiometric UO_2 – UO_{2+x} – might be encountered at various stages of the nuclear fuel cycle if oxidative conditions are met; the impact of stoichiometry changes upon physical properties should therefore be properly assessed to ensure safe and reliable operations. These physical properties are intimately linked to the arrangement of atomic defects in the crystalline structure. The evolution of the defect concentration with environmental parameters – oxygen partial pressure and temperature – were evaluated by means of a point defect model where the reaction energies are derived from atomic-scale simulations. To this end, various configurations and net charge states of oxygen interstitial clusters in UO_2 have been calculated. Various methodologies have been tested to determine the optimum cluster configurations and a rigid lattice approach turned out to be the most useful strategy to optimize defect configuration structures. Ultimately, results from the point defect model were discussed and compared to experimental measurements of stoichiometry dependence on oxygen partial pressure and temperature.

Keywords

uranium dioxide, point defects, defect clustering, defect chemistry, deviation from stoichiometry

† Permanent address: emrecaglak@gmail.com

‡ Now at Federal Agency for Nuclear Control – FANC (Belgium)

1 Introduction

Over the past decades, uranium dioxide (UO_2) has been the reference fuel for the current fleet of nuclear reactors (Gen-II and Gen-III); today it is also considered by the Gen-IV International Forum for the first cores of the future generation of nuclear reactors on the roadmap towards minor actinide (MA) based fuel technology [1]. Thermodynamic and transport properties of UO_2 are a strong function of non-stoichiometry. Although a remarkable number of studies has been performed to address the relationship between the material properties and oxygen defects in UO_{2+x}, the fascinating complexity of these defects calls for further investigations [2–7].

it is widely known that the UO_2 lattice can host a large number of oxygen defects in various charge states and configurations, for example, by clustering with electronic defects, both electrons and holes; the only experimentally proven defect configuration is the di-interstitial cluster derived from neutron diffraction measurements by Willis [8]. Computer simulations techniques can help to get insight in these defect structures, considering that they can be addressed by density functional theory (DFT) or empirical potentials (EP) [9–14]. For such investigations it is of paramount importance to gain a quantitative knowledge of the defect concentrations as a function of environmental conditions, that is, temperature and oxygen potential (or oxygen partial pressure). This knowledge is provided by a point defect model (PDM) in which the chemical defect reactions are evaluated via a mass action law [15,16]. From that model, deviation from stoichiometry x in UO_{2+x} can be derived, which is also experimentally accessible.

Recent theoretical works, for example, Murphy et al., evaluated point defect concentrations and non-stoichiometry in thoria using DFT to predict the defect formation energies [17]. A similar approach was adopted for uranium oxide by Cooper et al., [9]. Soulié et al., [18] and Bruneval et al., [19] extended the UO_2 study by adding oxygen defect clusters in their model. Even though, their results qualitatively provide a comparable defect concentration trend, the quantitative understanding still suffers from inconsistencies. This is mainly because of the various approximations used for the descriptions of the strong correlation between uranium *f* electrons, which in turn affects the defect formation energies. Unlike the above mentioned studies, we investigated the oxygen clusters up to di-interstitial by means of empirical potential simulations in expectation of qualitative agreement between DFT and EP. The positive results then further motivated us to go through a qualitative validation against measurements of stoichiometry dependence on oxygen partial pressure and temperature. In the future this will also allow us to discuss the solubility of different fission products and dopants in the UO_2 matrix at EP level.

2 Methods

2.1 Atomic scale simulations

Atomic scale simulations were performed using the LAMMPS software, version 2017 [20]. Calculations consider atoms as pointwise charged particles interacting with each other through interatomic potentials. These calculations were complemented with the GULP software in view of its ability to compute defect energies with different methods [21]. In order to maintain coherence, the system defect energy calculations were performed using the same interatomic potentials with both codes.

Several sets of parameters have been derived in the open literature to describe atom interactions for the UO_2 system [22,23]. They differ in the degree of covalence, or ionicity ξ, with $(0 < \xi \leq 1)$, attributed to ions and the analytical expression used for the short-range atom interactions. Most potentials are variants of the Buckingham potential form [24], sometimes coupled to a Morse term [25] to describe covalent bounds. The commonly adopted expression for the pair potential between ions i and j separated by distance $\mathrm{r_{ij}}$ takes the following form:

$$\mathrm{V}(\mathrm{r_{ij}}) = \frac{(\xi e)^2 \mathrm{Z_i Z_j}}{4\pi\epsilon_0 \mathrm{r_{ij}}} + \mathrm{A_{ij}} \exp\left(-\frac{\mathrm{r_{ij}}}{\rho_{\mathrm{ij}}}\right) - \frac{\mathrm{C_{ij}}}{\mathrm{r_{ij}^6}} + \mathrm{D_{ij}}[\exp\left(-2\gamma_{\mathrm{ij}}(\mathrm{r_{ij}^*} - \mathrm{r_{ij}})\right) - 2\exp(-\gamma_{\mathrm{ij}}(\mathrm{r_{ij}^*} - \mathrm{r_{ij}}))] \quad (1)$$

The first term stands for the electrostatic interaction between point charges with ϵ_0, the vacuum permittivity. For UO_2, one considers full ionicity: $\mathrm{Z}(\mathrm{U}^{4+}) = +4$ and $\mathrm{Z}(\mathrm{O}^{2-}) = -2$. Classical Ewald summation techniques were used to handle long-range electrostatic interactions in three dimensions. The second term of Eq. (1) expresses the short-range repulsion of overlapping electronic shells and the third term expresses the van der Waals attraction as a simple inverse power function. The last term is a Morse function that represents the covalent bond of the uranium-oxygen pairs. Pairwise interactions were evaluated up to a cut-off distance of 1.1 nm. The system configuration was relaxed at constant volume until a convergence of 10^{-4} eV is reached (total energy difference between consecutive minimisation steps).

Earlier studies revealed that the predictive character of empirical interatomic potentials for mechanical, thermal or defect properties of UO_2 are quite challenging, as there is no universal set of parameters [23,26–28]. While these studies generally addressed absolute values, the present work rather focuses on relative values, such as defect binding energies, for which better agreement was observed between interatomic potential parameter sets [29]. The Yakub potential has been extensively tested in literature for both static and dynamic calculations, and reproduces reasonably well defect and thermo-mechanical

properties of UO_2 [12,30,31]. This potential was therefore selected for this study; its short range parametrization is reported in Table 1.

Table 1 Short range parametrization of Yakub et al., [12]*, and* $\xi = 0.5552$

ion pairs	A_{ij} (eV)	$\rho_{ij} \times 10^{-10}$ (m)	$C_{ij} \times 10^{-60}$ (eV.m^6)	D_{ij} (eV)	$\gamma_{ij} \times 10^{10}$ (m^{-1})	$r_{ij}^* \times 10^{-10}$ (m)
U^{4+}-O^{2-}	432.18	0.3422	0.0	0.5055	1.864	2.378
U^{4+}-U^{4+}	187.03	0.3422	0.0	0.0	-	-
O^{2-}-O^{2-}	883.12	0.3422	3.996	0.0	-	-

In UO_2, hole electronic defects are generally thought to maintain the system charge neutral [32]. In the present study, holes were described as localised on the uranium sublattice as uranium atoms with a (5+) charge. For the description of interactions involving those particles the atom charge (Z) is simply modified while respecting the ionicity proposed in the original model – see Eq (1). Modifications of the short-range interactions were considered as a second order effect and were not applied for this study [29,33,34].

2.2 Defect calculations

Defect calculations were performed according to the supercell method, with LAMMPS [20], where a pristine system of 4 x 4 x 4 conventional UO_2 unit-cells under periodic boundary conditions was considered as a starting structure [22]. The lattice parameter was set to the experimental value for UO_2, 0.547 nm [35], before relaxation. Defects were introduced in the system, which is then relaxed to find the energy minimum, and the corresponding atomic configuration.

Reaction energies are based on the system energy difference between the individual products and reactants. One must remain careful when interpreting the as-calculated energies in empirical potential calculations, as only energy differences between systems having an identical set of particles have a straightforward, physical, meaning. For the defect calculations that do not preserve the stoichiometry of the pristine material – where particles of one or several species[2] appear in or disappear from the system – the calculated defect energy implicitly takes, as a reference state for that particle, the non-interacting, charged, particle in vacuum. For example, in the case of an oxygen interstitial defect, the reference states consist of the pristine UO_2 crystal on the one hand, and a charged O^{2-} in vacuum on the other hand. The latter configuration is purely conceptual in the empirical potential method, as the second electron captured actually remains unbound in vacuum.

[2] one also considers here atoms with different charges as different species.

To overcome this issue, one focuses here on stoichiometric defect reactions (that conserve the species), so that the corrections for particle addition and removal cancel out. Coming back to our example, neither the as-calculated oxygen interstitial energy, neither the opposite defect – the oxygen vacancy – energy, have a physical meaning. However, when combining the results, one obtains the oxygen Frenkel pair energy. In order to facilitate the construction of a point defect model from empirical potential calculations, one privileges defect reactions expressing the formation of defect clusters from their individual components, i.e. evaluating the free energy change.

At EP level, issues remain for some of the reactions considered in the PDM, (see § 2.4); for example the formation of an electron-hole pair, for which the electron and hole tend to be localised on the uranium sublattice. The creation of the pair implies the disappearance of two regular U^{4+} atoms, and the apparition of one U^{3+} and one U^{5+} atom and, hence, a species change from empirical potential simulation perspectives. Empirical pair-potentials results need to be corrected for the difference in ionization energy between U^{3+} and U^{5+}, for example following a Born-Haber cycle [36]. Alternatively, a value derived from experiment [37] or *ab initio* calculations [38] could be used for the defect reaction energy.

For the system oxidation reaction, no proper correction scheme exists, as it would involve the calculation of an O_2 molecule. The latter state is far from the validation domain of the empirical potentials used, considering that they were developed to address ceramic crystals. For that reaction, energies derived from experiment [39] or *ab initio* calculations would be a better alternative [14].

The supercell method can be applied to a charged system, such as for defect calculations. A neutral system is recovered by adding a uniform background charge to the system [40], whereas this correction is not implemented in LAMMPS. This background charge does not affect interatomic forces and simply results into an additional term to the system total energy. At post-processing, defect energies are then corrected for the charge's Madelung energy to the infinite dilution limit according to the potential predictions: $f^{\infty} = f^{\mathrm{L}} + \frac{\mathrm{q}^2\alpha}{2\epsilon \mathrm{L}}$ where f^{∞} and f^{L} is a formation energy of the defect at infinite dilution and under periodic boundary conditions with total system size L (=0.544 x 4 nm after relaxation of the pristine system), q is the total charge on the solid, α (=2.84) is the cubic system Madelung constant and ϵ (=3.28, for Yakub [12] potential) is the static dielectric constant.

2.3 Exploration of configuration space

The charge state of oxygen interstitials (O_i) and O_i clusters is evaluated in this empirical potential study. One also considers the presence of charge-compensating holes that would be bound to the defect. The exploration of the arrangement of holes around a single oxygen interstitial defect, or an oxygen interstitials cluster, is a difficult task, considering that the number of cases to be addressed increases in a combinatorial way with the number of holes considered: $\frac{N!}{(N-n)!n!}$, with N, the number of accessible sites (256) for a 4 x 4 x 4 unit-cell system, and n, the number of U^{5+} inserted in the system. In order to optimize the calculation time, several methods were tested.

- The brute force approach, used as a reference, where all possible combinations are relaxed and compared in terms of energy. The method only performs in a reasonable amount of time for up to three U^{5+} in the system (~2.7×10^6 combinations).
- A Monte-Carlo approach was then tested, similar to former works [41–43], where U^{5+} are only displaced when the energy gain after the displacement obeys an acceptance (Metropolis) criterion. The major issue with this approach is that one generally starts from a relaxed configuration, so that the permutation of an U^{5+} and an U^{4+} ions most often results in a positive energy gain. Although well-thought criteria enable to progressively converge towards lower energy configurations, convergence to the energy minimum is slow and not guaranteed.
- A rigid lattice approach, where one considers that the non-relaxed and the relaxed configuration maps are qualitatively similar. The search for the optimal configuration is performed in the non-relaxed system (1st stage) and the optimal configuration is relaxed (2nd stage). By doing so, one avoids repeated relaxation stages, which each necessitate of the order of 100 to 1000 calculation steps. The relaxed configuration energy is only calculated once, for the optimal configuration. Although the method could be used in brute-force scheme, the interest also lies in coupling it to a Monte-Carlo algorithm; the fact that non-relaxed configurations are used eliminates the energy gain issue evoked previously when permuting U^{5+} with U^{4+} ions.

The latter approach was validated for the clustering of a single oxygen interstitial with one and two holes and compared to a brute force approach. Both methods converged towards the same geometrical arrangement. In the case of a single hole, the hole is predicted to occupy a first nearest neighbour position relative to the oxygen interstitial. With two holes, the predicted configuration of minimum energy consisted of the holes located in second nearest neighbour positions to the oxygen interstitial, as illustrated by the mapping in Figure 1. They were located in opposite directions from each other, as

could be expected from pure electrostatic considerations; that configuration is also in good agreement with recent DFT calculations [44].

The systematic configuration space exploration confirmed that the minimum energy configuration was indeed reached. The rigid lattice approach was thus observed to rapidly converge towards the optimal configuration found with the brute approach method. Based on the computing time gain and efficiency performance – convergence to the energy minimum is observed after about 5000 Monte-Carlo swaps –, the method is expected to facilitate the search for optimum configurations when a larger number of defects are at play.

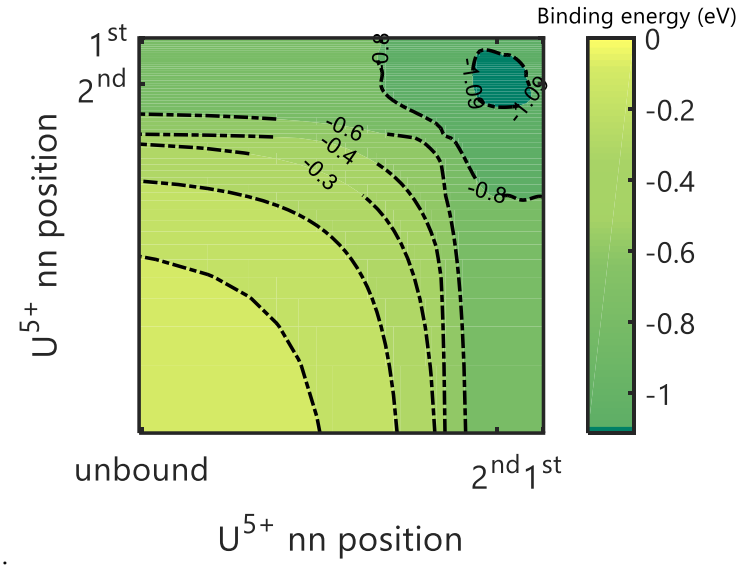

Figure 1 Binding energy of two holes and an oxygen interstitial atom as predicted with Yakub potential [12] *. The contour map expresses the binding energy as a function of the distance of each hole to the oxygen interstitial atom. When different configurations correspond to the same distances, the minimum value over these configurations is retained. The most stable configuration is observed for both holes located in second nearest neighbour to the oxygen interstitial, in opposite direction (along <1 1 1> direction) from each other as it is shown in Figure 2.*

2.4 Point defect model

A point defect model (PDM) expresses interactions (or reactions) between defects in a similar way as one treats chemical reaction equilibria. It links, for each reaction, the concentrations at equilibrium of the species involved. Although virtually any defect and defect reaction could be considered, the point defect model will only provide a good representation of a material if the dominant defects are included in the picture. In uranium dioxide, it is commonly accepted that the dominant defects relate to electronic and oxygen disorder [45,46]. The simplest description of UO_2, close to stoichiometry, expresses the polaron (electron-hole pair creation) and the oxygen Frenkel (oxygen vacancy – interstitial pair) equilibria. Using Kröger-Vink notations [15], these reactions can be expressed, respectively as:

$$2U_U^{\times} \rightleftharpoons U_U^{\bullet} + U_U' \quad (2)$$

$$v_i^{\times} + O_o^{\times} \rightleftharpoons O_i'' + v_o^{\bullet\bullet} \quad (3)$$

A relation between defect concentrations may then be expressed according to the mass action law which involves the change in free energy of the system Δf:

$$K_D = \frac{[U_U'][U_U^{\bullet}]}{[U_U^x]^2} = \exp\left(-\frac{\Delta f^D}{k_B T}\right) \quad (4)$$

$$K_F = \frac{[O_i''][v_o^{\bullet\bullet}]}{[O_o^x][v_i^x]} = \exp\left(-\frac{\Delta f^F}{k_B T}\right) \quad (5)$$

Where $[U_U^{\bullet}]$ and $[U_U']$ are the concentration of holes and electrons assumed in the valence and conduction band, respectively [47]. $[O_i'']$ represents the interstitial oxygen concentration while $[v_o^{\bullet\bullet}]$ is the oxygen vacancy concentration. This simple system expressed by Eq. (2) and (3) contains seven unknowns and needs to be closed by other relations that express, for example, conservation of the site occupancy and of the system charge neutrality. In the infinite dilution limit, one may approximate regular atom concentrations by their value in a perfect crystal $[U_U^{\times}] \approx [v_i^{\times}] \approx \frac{1}{2}[O_O^{\times}] \approx 1$ otherwise the relative contribution of each defect to uranium, oxygen and interstitial lattices should be summed up. The charge neutrality condition for defects (i) with a concentration C_i and net charge q_i must be maintained:

$$\sum_i q_i C_i = 0 \quad (6)$$

One last relation is required, which links the system to the constraints imposed by the environment. For UO_2, we consider that the oxidation reaction from the atmosphere surrounding the system dominates. The point defect reaction is expressed as:

$$v_i^{\times} + 2U_U^{\times} + \frac{1}{2}O_2(g) \rightleftharpoons O_i'' + 2U_U^{\bullet} \quad (7)$$

Or, in mass action law form:

$$K_O = \frac{[O_i''][U_U^{\bullet}]^2}{[U_U^x]^2[v_i^x]\sqrt{p_{O_2}}} = \exp\left(-\frac{\Delta f^O}{k_B T}\right) \quad (8)$$

Where p_{O_2} stands for the surrounding oxygen partial pressure. The deviation from stoichiometry x, in a regime dominated by isolated oxygen interstitials and holes, follows $\propto p_{O_2}^{1/6}$. This simple description of defects in UO_2, however, does not correspond to what is experimentally observed at larger deviation from stoichiometry; it has been evidenced that a better picture is provided if the clustering of oxygen

interstitials is accounted in the model, as the observed relation rather obeys $x \propto p_{O_2}^{1/2}$[48–50]. One therefore introduces oxygen interstitial clusters with varying effective charges in the point defect model. Changes in the defect cluster charge were modelled in this work through the presence of localised holes on the uranium site. Assuming that a single individual oxygen interstitial cluster species dominates, in the form of $\{nO_i'': pU_U^{\bullet}\}^{(2n-p)'}$ – with n, the number of oxygen interstitials and p, the number of holes in the cluster – the corresponding power dependency for the charge neutral system could be generalised as $x \propto p_{O_2}^{m}$, with the exponent $m=\frac{n}{2(2n-p+1)}$. For example, in the case of isolated O_i'' (n=1, p=0) one comes back to the first case and $m=\frac{1}{6}$; this situation is expected to dominate close to perfect stoichiometry when clustering is not favourable for configurational entropy reasons. Experimentally, one observes a domain where the power dependency of x goes as $p_{O_2}^{1/2}$; this observation would be compatible with two clusters of limited size: $\{Oi'': 2U_U^{\bullet}\}^{x}$ (n=1, p=2) or $\{2Oi'': 3U_U^{\bullet}\}'$ (n=2, p=3). Stoichiometry measurements can not distinguish between the two types of clusters. Electrical conductivity will, however, be sensitive to the type of defect, since the latter defect cluster type needs to be compensated by non-bound holes, which are mobile, while the former cluster type is fully charge compensated. Several authors have proposed to consider singly charged di-interstitial clusters as the dominant defect at moderate departures from stoichiometry [48–50]. This leads to:

$$nO_i'' + p\,U_U^{\bullet} \rightleftharpoons \{nO_i'': pU_U^{\bullet}\}^{(2n-p)'} \quad (9)$$

$$K_{Cls.} = \frac{[\{nO_i'': pU_U^{\bullet}\}^{(2n-p)'}]}{[Oi'']^n[U_U^{\bullet}]^p} = \exp\left(-\frac{\Delta f^{Cls.}}{k_B T}\right) \quad (10)$$

If one assumes that next to isolated point defects, only di-interstitial clusters with charge -1 are formed, the site balances may be expressed as:

$$[U_U^{x}] + [U_U^{\bullet}] + [U_U'] = 1 \quad (11)$$

$$[O_o^{x}] + [v_o^{\bullet\bullet}] = 2 \quad (12)$$

$$[v_i^{x}] + [O_i''] + (2+a)[\{2O_i'': 3U_U^{\bullet}\}'] = 1 \quad (13)$$

The parameter a is used here for $\{2O_i'': 3U_U^{\bullet}\}'$ or Willis clusters to restrict access to neighbour interstitial sites. Using $a \approx 6$ also enables to reproduce UO_{2+x} saturation at x=0.25, i.e. a stoichiometry corresponding to U_4O_9. The PDM system of equations is solved with a Newton-Raphson iterative technique, ensuring numerical convergence is obtained. The deviation from stoichiometry is then evaluated from the various defect concentrations, considering that defects on the uranium sub-lattice play a negligible role:

$$x = |\sum n[\{nOi'': pU_U^{\bullet}\}^{(2n-p)'}] - [v_o^{\bullet\bullet}]| \quad (14)$$

3 Results and Discussions

3.1 Oxygen interstitial clusters configuration and energy

The configuration and the defect energy was calculated for various cluster of oxygen interstitials and holes by means of the rigid lattice approach to determine the lowest energy structure (cf. §2.3). All the defect configurations were rendered in Figure 2 and defect energies were listed in Table 2.

Clusters involving a single oxygen interstitial and one or two holes has already been addressed in § 2.3. While the single hole is predicted to bind as first nearest neighbour to the oxygen interstitial, the most stable defect arrangement with two holes consists of these holes located in second nearest neighbour positions to the oxygen interstitial, in opposite directions from each other. That configuration is in agreement with DFT calculations [44].

Di-interstitial clusters were studied here as charge-compensated clusters, with one to four holes. The most stable arrangement of two oxygen interstitial atoms was first determined separately due to it exhibiting a metastable state; the presence of charge-compensating holes was considered in a second stage; two oxygen interstitials were initially placed in two nearest octahedral interstitial site with a separation of $\frac{\sqrt{2}}{2}$ times lattice parameter. Figure 2 shows the optimal arrangement of two oxygen interstitials $\{2O_i''\}''''$, as predicted in this study. We then investigated complex di-interstitial defect clusters with varying charges $\{2O_i'': pU_U^{\bullet}\}^{(4-p)\prime}$. For a single charge-compensating hole $\{2O_i'': U_U^{\bullet}\}'''$, the most stable configuration consists of the hole located on one of the closest neighbours of the oxygen interstitials. The structure of the $\{2O_i'': 2U_U^{\bullet}\}''$and $\{2O_i'': 3U_U^{\bullet}\}'$ clusters, however, do not correspond to the traditional description from Willis, with two regular oxygen atoms displaced from their regular position [8]. While uranium ions are not displaced from their regular fluorite location, an alternative arrangement of the oxygen atoms was predicted here, where oxygen atoms stabilize as a split di-interstitial $\{3Oi'': v_O^{\bullet\bullet}\}$. In such a configuration, oxygen ions are arranged as a regular triangle, with positions along <111> directions from a central oxygen vacancy. This structure, with a single oxygen atom displaced from its regular position was also derived in DFT calculations [38].

Our study predicted the progressive binding of the cluster as it accumulates one, two and three holes, but the neutral cluster, with 4 holes, tended to be less stable. Without further interpretation through a point defect model at this stage, this result already suggests that from pure energy perspectives, di-interstitial clusters of charge -1 could be encountered, as often suggested from interpretation of experimental data through point defect models. The results also suggest a low probability of forming neutral di-interstitial clusters.

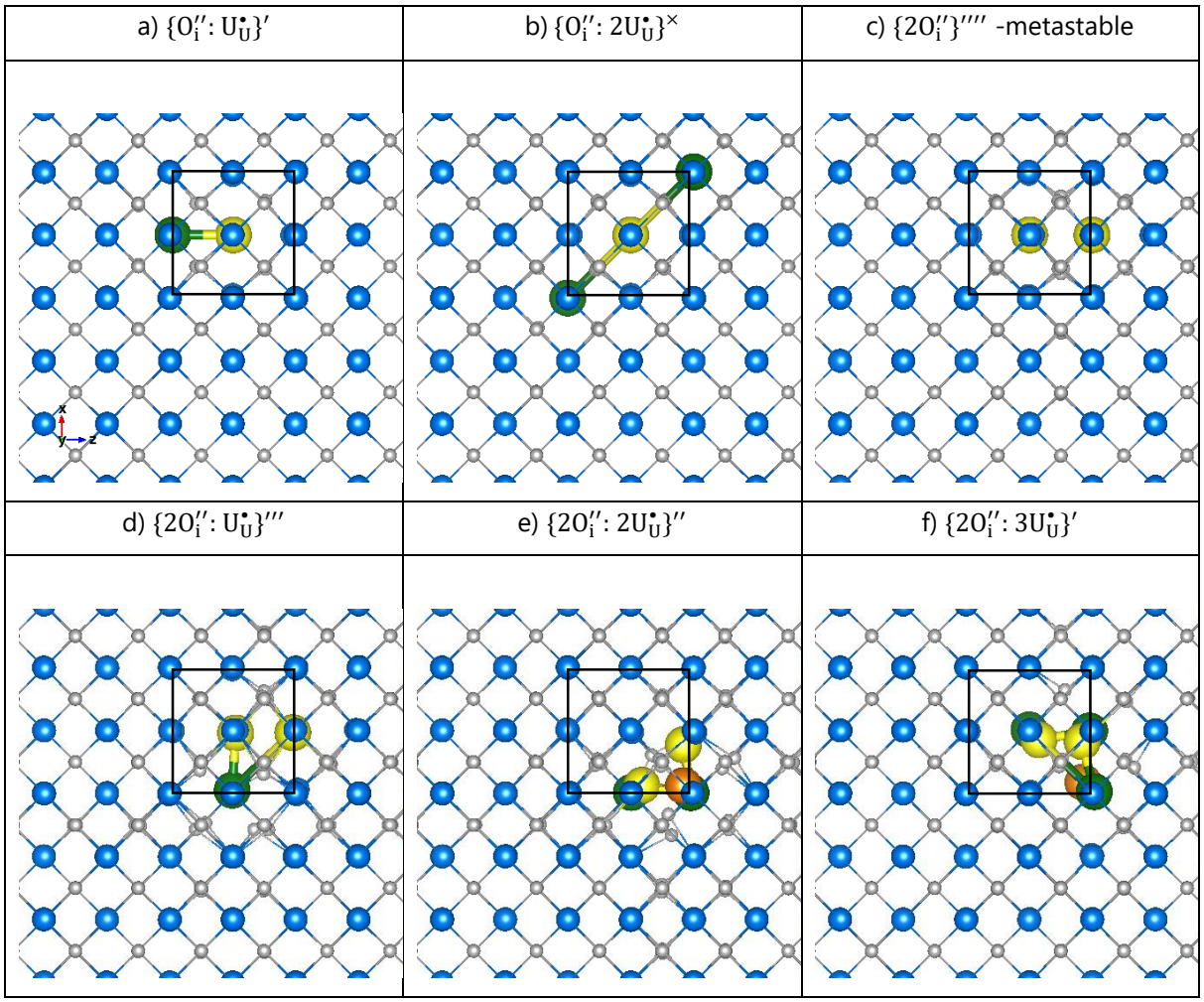

Figure 2 Yakub potential relaxed configurations of oxygen interstitial and interstitial clusters [12]. *Blue and white spheres represent the regular uranium and oxygen ions in f.c.c. UO_2. Yellow spheres stand for interstitial oxygen ions while the green ones for U^{5+} (holes) positions. For the case $\{2O_i'': 2U_U^{\bullet}\}''$ and $\{2O_i'': 3U_U^{\bullet}\}'$ orange spheres are used to highlight oxygen ions displaced from their regular positions. For the sake of clarity, central vacancy sites are not emphasized.*

Once the most stable defect cluster configurations were obtained with LAMMPS [20], they were further analysed in terms of their energies with GULP [4]. Using the GULP code, the supercell method results were cross-checked with values derived using the Mott and Littleton approach [51] . The latter method divides the space around the defect into three regions; in region I atoms are fully relaxed, while in region IIa, only harmonic relaxation due to the defect charge is assumed; in Region IIb, an infinite purely dielectric medium is assumed. In this work, we used radii of 1.4 nm for region I and 2.8 nm for region IIa; very good agreement between both methods is generally reported [52,53] and also observed here. Results of binding energy calculations in the supercell approach are reported in Table 2.

Table 2 Prediction of the defect clustering binding energy $\Delta f^{Cls.}$, in uranium dioxide calculated with 4 x 4 x 4 unit-cell method using Yakub potential [12] *. Negative binding energy indicates preference for the cluster over its individual components.*

Binding Energy	$\{O_i'': U_U^{\bullet}\}'$	$\{O_i'': 2U_U^{\bullet}\}^{\times}$	$\{2O_i''\}''''$	$\{2O_i'': U_U^{\bullet}\}'''$	$\{2O_i'': 2U_U^{\bullet}\}''$	$\{2O_i'': 3U_U^{\bullet}\}'$
$\Delta f^{Cls.}$ [eV]	-0.67	-1.09	1.26	-0.12	-1.40	-2.09

3.2 Deviation from stoichiometry

Point defects energies were evaluated for UO_{2+x} (see in Table 2). They were complemented with a PDM in which the defect concentrations were derived from the reaction energies. We assume that the system of Eq. (4), (5) and (8) dominates at exact stoichiometric composition and they may be solved analytically under the following assumptions: $[O_i''] = [v_o^{\bullet\bullet}]$, $[U_U^{\bullet}] = [U_U']$ and the $[U_U^{\times}] \approx [v_i^{\times}] \approx \frac{1}{2}[O_O^{\times}] \approx 1$. For such a case, K_O is expressed as:

$$K_O = K_D \sqrt{\frac{2 \times K_F}{p_{O_2}^*}} \qquad 15$$

The oxygen partial pressure at exact stoichiometry $p_{O_2}^*$, suffers from large discrepancies between laboratories [35,48,54,55]. One of the reasons might be that the samples exhibit different impurity contents. Measurements performed by Leinders et al., [35] concluded that the relation found by Lindemer and Besmann's [54] data analysis gives the best agreement with their observations. In spite of the inconsistencies, we used the Lindemer and Besmann predictions for both $p_{O_2}^*$ vs temperature (T) and the x in UO_{2+x} vs $p_{O_2}^*$ [54]. This allows us to implicitly handle the defect vibrational entropies as corrections to K_O.

Another parameter appearing in Eq. (15) is K_D which is related to the band gap energy. *Ab initio* calculations and experiments generally agree on the band gap width – the energy to form an electron in the conduction band and a hole in the valence band –, with Δf^{D} =2.1+/-0.1 eV [37,38].

It was observed that reaction constant K_O in Eq. (15) is ultimately linked to the precision of K_F, $p_{O_2}^*$ and K_D. Any changes in those parameters would significantly affect the overall defect concentrations. Two recent studies report and discuss inconsistencies between the Frenkel pair energy –related to K_F - derived from atomic scale simulations and experiments [22,31]. One reports an experimental range of 3 – 4.6 eV [2,56] while atomistic simulations (both *ab initio* and EP) generally predict slightly higher values, i.e. between 3 – 7 eV [22,31,57]. The Yakub potential provides a value of 5.7 eV [12].

In a first phase, the stoichiometric deviation of UO_2 was qualitatively evaluated. Eq. (15) was used to calculate K_O with the normalised pressure at exact stoichiometry i.e. $p_{O_2}/\ p^*_{O_2}$ =1. Results presented in Figure 3 show that isolated oxygen interstitials O_i'' dominate at lower oxygen partial pressure region in UO_{2+x}. No significant contribution was observed from other types of single interstitial clusters, namely: $\{O_i'': U_U^{\bullet}\}'$ and $\{O_i'': 2U_U^{\bullet}\}^x$. The general concentration trend for single interstitial clusters at lower partial pressure $[O_i^{''}]$ > $[\{O_i'': U_U^{\bullet}\}']$ > $[\{O_i'': 2U_U^{\bullet}\}^x]$ was determined which is also in line with the interpretation of DFT simulation results [9]. They all progressively saturate as one approaches x~0.07, considering that beyond that value, first neighbour sites would become populated; then oxygen interstitials cannot be considered as isolated anymore. In the case of di-interstitial clusters, the trend predicted at higher oxygen partial pressure is to observe single charge di-interstitial clusters dominating: $[\{2O_i'': 3U_U^{\bullet}\}']$ > $[\{2O_i'': 2U_U^{\bullet}\}'']$ > $[\{2O_i'': U_U^{\bullet}\}''']$ > $[\{2O_i''\}'''']$. Therefore, once higher order clustering is a concern, non-formally charged defects were observed to dominate. Considering saturation of isolated oxygen interstitial clusters occurs at low departure from stoichiometry because of site exclusion – if a first neighbour site becomes occupied, a di-interstitial cluster is actually formed – one focuses on a relatively simple PDM made of isolated point defects and a single type of oxygen interstitials clusters $[\{2O_i'': 3U_U^{\bullet}\}']$, which was predicted in this study to dominate at higher stoichiometry.

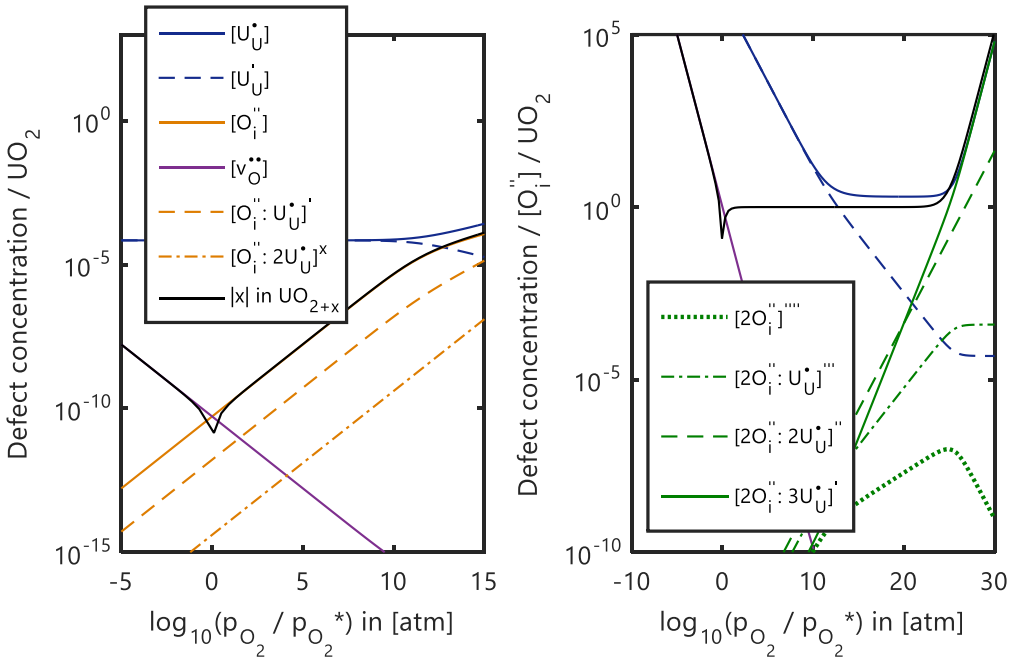

Figure 3 Qualitative evaluation of defect concentrations in UO_{2+x} predicted by Yakub potential [12]. *Left) represents the single interstitial clustering concentrations and Right) is di-interstitial clustering concentrations over the normalised oxygen pressure range at 1273 K.*

In a second phase, Eq. (15) was used to calculate K_O with the oxygen pressure at exact stoichiometry provided by Lindemer and Besmann [54]. We considered the general agreement on the band gap and on the overestimation of the Frenkel pair energy by empirical potential simulations, which was described earlier. The dependence of K_O to K_F was also derived from the Lindemer and Besmann's work on the basis of Eq. (15) [54]. The calculated Frenkel pair energy Δf^F, and oxidation reaction energy Δf^O are reported in Table 3. These energies have been found to be in good agreement with literature values.

Table 3 Calculated Frenkel pair energy Δf^F, and Oxidation reaction energy Δf^O.

Formation Energy	This study	Other works
Δf^F [eV]	4.1+/-0.1	3.0 to 4.6 [2,56]
Δf^O[eV]	-0.4+/-0.01	-0.2 to -0.8 [3,6]

The defect concentrations as a function of oxygen partial pressure were computed at equilibrium for UO_{2+x} and presented at three different temperatures (see Figure 4). The material stoichiometry was then derived from the oxygen defect balance. As illustrated in these Figures, the agreement for the departure from stoichiometry at approximately $x \leq 0.01$ suffers from large uncertainties, which should be put into perspective with the large experimental uncertainty at these low values of x. At higher pressure, predictions on the x in UO_{2+x} fits well with the experimental data points show better agreement for the x in UO_{2+x}.

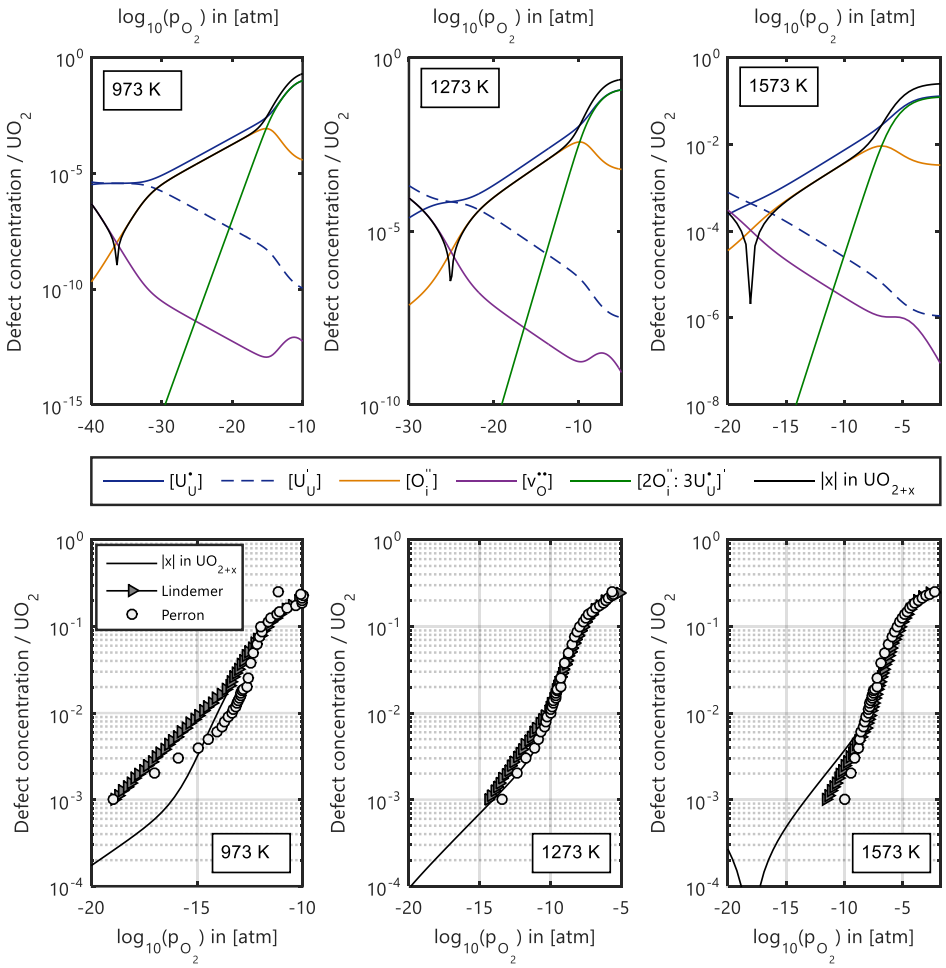

Figure 4 The deviation from stoichiometry x in UO2+x (bottom row) is calculated from the defect concentrations over a range of temperatures (top row). Comparison is made with the correlations published by Lindemer and Besmann [54]*, and Perron's thermodynamic data,*[55].

4 Conclusions

The clustering behaviour of oxygen interstitials and holes is addressed by empirical potential based atomic scale simulations. The defect energies are then interpreted by mean of a PDM to derive the concentration of defects and defect clusters as a function of temperature and oxygen partial pressure. A validation of the methodology and the results is conducted on the basis of the deviation from stoichiometry in UO_{2+x}.

The following results were achieved:

- Configurational space exploration of the arrangement of localised holes around isolated oxygen interstitials and oxygen interstitial clusters was shown to be most effective with a combination of a rigid lattice approach – where no relaxation is performed in a first stage – with a Metropolis Monte Carlo particle swapping method.

- The PDM established from EP results and experimental values which are not accessible to EP techniques shows good agreement with various sets of experimental data.
- With the proposed dominant defect type -$\{2O_i'' : 3U_U^{\bullet}\}'$, di-interstitial with minus one charge-, the calculated relation between both stoichiometry and electrical conductivity evolution with oxygen partial pressure have a power dependence that corresponds to what was shown in experiments. Especially, at 1273 K and 1573 K good agreement between our model and experiments was achieved.
- At 973 K, both the experiments and the proposed model show slight inconsistencies. One might also consider that at low temperature (<600 K) UO_2 exhibits a solid solution with U_4O_9 in which the excess oxygen ions agglomerate into a cuboctahedron (CoT) structure [58–60]. Such a clustering configuration of higher order might dominate the deviation from stoichiometry in UO_{2+x} at low temperature. However, this statement is based solely on theoretical arguments and not supported by experimental data; it should therefore be addressed in future work.

5 Acknowledgements

This work is dedicated to the memory of Prof. Alain Dubus, ULB, Bruxelles, Belgium. Financial support from the SCK CEN is gratefully acknowledged.

6 Data availability

The data that support the findings of this study are available from the corresponding author, E.C., upon reasonable request.

7 References

[1] C. Behar, Technology roadmap update for generation IV nuclear energy systems, in: OECD Nucl. Energy Agency Gener. IV Int. Forum, 2014: pp. 2003–2014.

[2] H. Matzke, Atomic transport properties in UO 2 and mixed oxides (U, Pu) O 2, J. Chem. Soc. Faraday Trans. 2 Mol. Chem. Phys. 83 (1987) 1121–1142.

[3] A. Nakamura, T. Fujino, Thermodynamic analysis on point defects of UO2+ x at relatively small deviation from stoichiometry between 600 and 1400° C, J. Nucl. Mater. 140 (1986) 113–130.

[4] IAEA, Thermodynamic and transport properties of uranium dioxide and related phases, 1965.

[5] C. Guéneau, A. Chartier, L. Van Brutzel, Thermodynamic and thermophysical properties of the actinide oxides, (2012).

[6] P. Garcia, E. Pizzi, B. Dorado, D. Andersson, J.-P. Crocombette, C. Martial, G. Baldinozzi, D. Siméone, S. Maillard, G. Martin, A defect model for UO2+ x based on electrical conductivity and deviation from stoichiometry measurements, J. Nucl. Mater. 494 (2017) 461–472.

[7] D.A. Andersson, T. Watanabe, C. Deo, B.P. Uberuaga, Role of di-interstitial clusters in oxygen transport in UO 2+ x from first principles, Phys. Rev. B. 80 (2009) 60101.

[8] B.T.M. Willis, The defect structure of hyper-stoichiometric uranium dioxide, Acta Crystallogr. Sect. A Cryst. Physics, Diffraction, Theor. Gen. Crystallogr. 34 (1978) 88–90.

[9] M.W.D. Cooper, S.T. Murphy, D.A. Andersson, The defect chemistry of UO2±x from atomistic simulations, J. Nucl. Mater. 504 (2018) 251–260.

[10] P. Nerikar, T. Watanabe, J.S. Tulenko, S.R. Phillpot, S.B. Sinnott, Energetics of intrinsic point defects in uranium dioxide from electronic-structure calculations, J. Nucl. Mater. 384 (2009) 61–69.

[11] R.A. Jackson, A.D. Murray, J.H. Harding, C.R.A. Catlow, The calculation of defect parameters in UO2, Philos. Mag. A. 53 (1986) 27–50.

[12] E. Yakub, C. Ronchi, D. Staicu, Computer simulation of defects formation and equilibrium in non-stoichiometric uranium dioxide, J. Nucl. Mater. 389 (2009) 119–126.

[13] C.R.A. Catlow, Point defect and electronic properties of uranium dioxide, Proc. R. Soc. London. A. Math. Phys. Sci. 353 (1977) 533–561.

[14] D.A. Andersson, G. Baldinozzi, L. Desgranges, D.R. Conradson, S.D. Conradson, Density functional theory calculations of UO2 oxidation: Evolution of UO2+ x, U4O9–y, U3O7, and U3O8, Inorg. Chem. 52 (2013) 2769–2778.

[15] F.A. Kröger, H.J. Vink, Relations between the concentrations of imperfections in crystalline solids, in: Solid State Phys., Elsevier, 1956: pp. 307–435.

[16] F.A. Kröger, The chemistry of imperfect crystals, North-Holland Pub. Co.;, 1964.

[17] S.T. Murphy, M.W.D. Cooper, R.W. Grimes, Point defects and non-stoichiometry in thoria, Solid State Ionics. 267 (2014) 80–87.

[18] A. Soulié, F. Bruneval, M.-C. Marinica, S. Murphy, J.-P. Crocombette, Influence of vibrational entropy on the concentrations of oxygen interstitial clusters and uranium vacancies in nonstoichiometric U O 2, Phys. Rev. Mater. 2 (2018) 83607.

[19] F. Bruneval, M. Freyss, J.-P. Crocombette, Lattice constant in nonstoichiometric uranium dioxide

from first principles, Phys. Rev. Mater. 2 (2018) 23801.

[20] S. Plimpton, Fast parallel algorithms for short-range molecular dynamics, J. Comput. Phys. 117 (1995) 1–19.

[21] J.D. Gale, GULP: A computer program for the symmetry-adapted simulation of solids, J. Chem. Soc. Faraday Trans. 93 (1997) 629–637.

[22] K. Govers, S. Lemehov, M. Hou, M. Verwerft, Comparison of interatomic potentials for UO2. Part I: Static calculations, J. Nucl. Mater. 366 (2007) 161–177.

[23] S.I. Potashnikov, A.S. Boyarchenkov, K.A. Nekrasov, A.Y. Kupryazhkin, High-precision molecular dynamics simulation of UO2–PuO2: Pair potentials comparison in UO2, J. Nucl. Mater. 419 (2011) 217–225.

[24] R.A. Buckingham, The classical equation of state of gaseous helium, neon and argon, Proc. R. Soc. London. Ser. A. Math. Phys. Sci. 168 (1938) 264–283.

[25] P.M. Morse, Diatomic molecules according to the wave mechanics. II. Vibrational levels, Phys. Rev. 34 (1929) 57.

[26] K. Govers, S. Lemehov, M. Hou, M. Verwerft, Comparison of interatomic potentials for UO2: Part II: Molecular dynamics simulations, J. Nucl. Mater. 376 (2008) 66–77.

[27] C.L. Bishop, R.W. Grimes, D.C. Parfitt, Establishing the isotropy of displacement cascades in UO2 through molecular dynamics simulation, Nucl. Instruments Methods Phys. Res. Sect. B Beam Interact. with Mater. Atoms. 268 (2010) 2915–2917.

[28] R. Devanathan, J. Yu, W.J. Weber, Energetic recoils in UO 2 simulated using five different potentials, J. Chem. Phys. 130 (2009) 174502.

[29] K. Govers, S.E. Lemehov, M. Verwerft, On the solution and migration of single Xe atoms in uranium dioxide–An interatomic potentials study, J. Nucl. Mater. 405 (2010) 252–260.

[30] T. Arima, K. Idemitsu, Y. Inagaki, Y. Tsujita, M. Kinoshita, E. Yakub, Evaluation of melting point of UO2 by molecular dynamics simulation, J. Nucl. Mater. 389 (2009) 149–154.

[31] S.I. Potashnikov, A.S. Boyarchenkov, K.A. Nekrasov, A.Y. Kupryazhkin, High-precision molecular dynamics simulation of UO2–PuO2: Anion self-diffusion in UO2, J. Nucl. Mater. 433 (2013) 215–226.

[32] A. Baena, T. Cardinaels, K. Govers, J. Pakarinen, K. Binnemans, M. Verwerft, Lattice contraction and lattice deformation of UO2 and ThO2 doped with Gd2O3, J. Nucl. Mater. 467 (2015) 135–

143.

[33] C.R.A. Catlow, Point Defect and Electronic Properties of Uranium Dioxide, Proc. R. Soc. London A Math. Phys. Eng. Sci. 353 (1977) 533–561.

[34] R. Ngayam-Happy, M. Krack, A. Pautz, Effects of stoichiometry on the defect clustering in uranium dioxide, J. Phys. Condens. Matter. 27 (2015) 455401.

[35] G. Leinders, T. Cardinaels, K. Binnemans, M. Verwerft, Accurate lattice parameter measurements of stoichiometric uranium dioxide, J. Nucl. Mater. 459 (2015) 135–142.

[36] J.D. Lee, Concise inorganic chemistry, John Wiley & Sons, 2008.

[37] J. Schoenes, Optical properties and electronic structure of UO2, J. Appl. Phys. 49 (1978) 1463–1465.

[38] J. Wang, R.C. Ewing, U. Becker, Average structure and local configuration of excess oxygen in UO 2+ x, Sci. Rep. 4 (2014) 4216.

[39] M.W. Finnis, A.Y. Lozovoi, A. Alavi, The oxidation of NiAl: What can we learn from ab initio calculations?, Annu. Rev. Mater. Res. 35 (2005) 167–207.

[40] M. Leslie, N.J. Gillan, The energy and elastic dipole tensor of defects in ionic crystals calculated by the supercell method, J. Phys. C Solid State Phys. 18 (1985) 973.

[41] J.A. Ball, M. Pirzada, R.W. Grimes, M.O. Zacate, D.W. Price, B.P. Uberuaga, Predicting lattice parameter as a function of cation disorder in MgAl2O4 spinel, J. Phys. Condens. Matter. 17 (2005) 7621.

[42] M.O. Zacate, R.W. Grimes, Combined Monte Carlo-energy minimization analysis of Al-Fe disorder in Ca2FeAlO5 brownmillerite, Philos. Mag. A. 80 (2000) 797–807.

[43] M.O. Zacate, R.W. Grimes, Simulation of Al/Fe disorder in Ca2FexAl2− xO5, J. Phys. Chem. Solids. 63 (2002) 675–683.

[44] B. Dorado, P. Garcia, G. Carlot, C. Davoisne, M. Fraczkiewicz, B. Pasquet, M. Freyss, C. Valot, G. Baldinozzi, D. Siméone, First-principles calculation and experimental study of oxygen diffusion in uranium dioxide, Phys. Rev. B. 83 (2011) 35126.

[45] B.T.M. Willis, Crystallographic studies of anion-excess uranium oxides, J. Chem. Soc. Faraday Trans. 2 Mol. Chem. Phys. 83 (1987) 1073–1081.

[46] Y. Ma, P. Garcia, J. Lechelle, A. Miard, L. Desgranges, G. Baldinozzi, D. Simeone, H.E. Fischer,

Characterization of Oxygen Defect Clusters in UO2+ x Using Neutron Scattering and PDF Analysis, Inorg. Chem. 57 (2018) 7064–7076.

[47] A.R. Massih, Electronic transport in pure and doped UO2, J. Nucl. Mater. 497 (2017) 166–182.

[48] P. Ruello, G. Petot-Ervas, C. Petot, L. Desgranges, Electrical conductivity and thermoelectric power of uranium dioxide, J. Am. Ceram. Soc. 88 (2005) 604–611.

[49] S.-H. Kang, J.-H. Lee, H.-I. Yoo, H.S. Kim, Y.W. Lee, Non-stoichiometry, electrical conductivity and defect structure of hyper-stoichiometric UO2+ x at 1000° C, J. Nucl. Mater. 277 (2000) 339–345.

[50] K. Park, D.R. Olander, A defect model for the oxygen potential of urania, High Temp. Sci. 29 (1990) 203–222.

[51] N.F. Mott, M.J. Littleton, Conduction in polar crystals. I. Electrolytic conduction in solid salts, Trans. Faraday Soc. 34 (1938) 485–499.

[52] R.A. Jackson, J.E. Huntingdon, R.G.J. Ball, Defect calculations in solids beyond the dilute limit, J. Mater. Chem. 1 (1991) 1079–1080.

[53] A. Walsh, A.A. Sokol, C.R.A. Catlow, Free energy of defect formation: Thermodynamics of anion Frenkel pairs in indium oxide, Phys. Rev. B. 83 (2011) 224105.

[54] T.B. Lindemer, T.M. Besmann, Chemical thermodynamic representation of UO2+x, J. Nucl. Mater. 130 (1985) 473–488.

[55] P.O. Perron, THERMODYNAMICS OF NONSTOICHIOMETRIC URANIUM DIOXIDE., Atomic Energy of Canada Ltd., Chalk River (Ontario), 1968.

[56] G.E. Murch, C.R.A. Catlow, Oxygen diffusion in UO 2, ThO 2 and PuO 2. A review, J. Chem. Soc. Faraday Trans. 2 Mol. Chem. Phys. 83 (1987) 1157–1169.

[57] M. Bertolus, M. Freyss, M. Krack, R. Devanathan, Assessment of current atomic scale modelling methods for the investigation of nuclear fuels under irradiation: Example of uranium dioxide, 2015.

[58] J.D. Higgs, B.J. Lewis, W.T. Thompson, Z. He, A conceptual model for the fuel oxidation of defective fuel, J. Nucl. Mater. 366 (2007) 99–128.

[59] D.J.M. Bevan, I.E. Grey, B.T.M. Willis, The crystal structure of β-U4O9− y, J. Solid State Chem. 61 (1986) 1–7.

[60] R.I. Cooper, B.T.M. Willis, Refinement of the structure of β-U4O9, Acta Crystallogr. Sect. A Found.

Crystallogr. 60 (2004) 322–325.